



Noninvasive thyroid histotripsy treatment: proof of concept study in a porcine model

John F. Swietlik, Scott C. Mauch, Emily A. Knott, Annie Zlevor, Katherine C. Longo, Xiaofei Zhang, Zhen Xu, Paul F. Laeseke, Fred T. Lee Jr. & Timothy J. Ziemlewicz

To cite this article: John F. Swietlik, Scott C. Mauch, Emily A. Knott, Annie Zlevor, Katherine C. Longo, Xiaofei Zhang, Zhen Xu, Paul F. Laeseke, Fred T. Lee Jr. & Timothy J. Ziemlewicz (2021) Noninvasive thyroid histotripsy treatment: proof of concept study in a porcine model, International Journal of Hyperthermia, 38:1, 798-804, DOI: [10.1080/02656736.2021.1922762](https://doi.org/10.1080/02656736.2021.1922762)

To link to this article: <https://doi.org/10.1080/02656736.2021.1922762>



© 2021 The Author(s). Published with license by Taylor & Francis Group, LLC



Published online: 26 May 2021.



[Submit your article to this journal](#)



Article views: 1311



[View related articles](#)





[View Crossmark data](#)



Citing articles: 1 [View citing articles](#)

Noninvasive thyroid histotripsy treatment: proof of concept study in a porcine model

John F. Swietlik^a , Scott C. Mauch^a, Emily A. Knott^a, Annie Zlevor^a, Katherine C. Longo^a, Xiaofei Zhang^b, Zhen Xu^c, Paul F. Laeseke^a, Fred T. Lee, Jr.^{a,d} and Timothy J. Ziemlewicz^a 

^aDepartment of Radiology, The University of Wisconsin, Madison, WI, USA; ^bDepartment of Pathology, The University of Wisconsin, Madison, WI, USA; ^cDepartment of Biomedical Engineering, The University of Michigan, Ann Arbor, MI, USA; ^dDepartment of Urology, The University of Wisconsin, Madison, WI, USA

ABSTRACT

Introduction: This study was performed to determine the feasibility and safety of creating superficial histotripsy treatment in a live porcine thyroid model.

Methods: The porcine thymus comparable in size, shape and location to the human thyroid was used for this study. This model has been used for thyroid surgery studies due to the diminutive size of the porcine thyroid. Four female swine underwent a total of eight histotripsy treatments performed with a prototype therapy system (HistoSonic, Inc., Ann Arbor, MI). Two treatments were performed in each animal: a spherical 1.0 × 1.0 × 1.0 cm and ovoid 1.0 × 1.0 × 2.0 cm treatment zones. MRI immediately post-procedure was evaluated for histotripsy treatment zone size and imaging appearance, followed immediately by sacrifice. Tissue was then reviewed for percent cellular destruction and precision.

Results: Treatment zones measured on post treatment MRI were similar to prescribed volumes (spherical = 0.60 (+/− 0.11) cm³, ovoid = 1.23 (+/− 0.40) cm³, $p > 0.05$ vs. prescribed). MRI demonstrated well demarcated treatment zones and imaging findings consistent with cellular destruction. Histology demonstrated sharp transitions to normal tissue (mean 0.33 (+/− 0.13) cm), and high degrees of cellular destruction (mean 76% (+/− 12.5), range of 50–100%) in the treated tissue. Edema within the overlying muscle was seen in 2/8 treatments.

Conclusion: Histotripsy is capable of safely creating precise histotripsy treatments within the superficial neck of a porcine thyroid model without evidence of considerable complications.

ARTICLE HISTORY

Received 25 November 2020

Revised 1 April 2021

Accepted 22 April 2021

KEYWORDS

Histotripsy; thyroid; noninvasive treatment

Introduction

Thyroid nodules are common in the adult population with an incidence of up to 68% [1–3]. The majority are benign and indications for treatment include symptom relief and improved cosmesis. Thyroid cancer is also common with 52,070 cases expected in 2019, but the relatively low number of associated deaths (3210 in 2019) denotes the indolent nature of the majority of cases [4]. Current national guidelines risk stratify thyroid nodules based on sonographic findings and size, and provide treatment recommendations [5]. However some nodules do not fit nicely into specific categories and their management can be open ended [5]. Surgical resection is the gold standard treatment for thyroid cancer and benign nodules requiring intervention [5–7]. A large number of thyroidectomy patients experience complications [8]. Prior studies have shown hypoparathyroidism and recurrent laryngeal nerve palsy in 25% and 7.5% of patients respectively both of which can substantially impact quality of life [9]. Post-operative bleeding is a life-threatening complication of thyroid surgery that can occur in 1–2% of patients [10]. More recently, minimally invasive ablation modalities

such as radiofrequency ablation (RFA), microwave ablation (MWA), percutaneous ethanol injection (PEI) and high intensity focused ultrasound (HIFU) have been used to treat both benign and malignant thyroid nodules [11–13]. Despite some success in decreasing the size of symptomatic and disfiguring benign nodules and early data suggesting efficacy in treating thyroid cancer, these treatments are associated with complications including skin burns, voice changes, shoulder drop, and hematomas [11–13]. A noninvasive, highly effective treatment option to reduce volume of benign nodules and treat thyroid cancer would be an important medical advance.

Histotripsy is a noninvasive, non-ionizing, non-thermal therapy, which uses short pulses of high amplitude focused ultrasound to produce cavitation and tissue destruction at the cellular level [14–16]. Histotripsy has been shown in pre-clinical models to create precise treatments with rapid resorption in multiple organs [17–22]. Yet the ability to create a treatment within the superficial anterior neck has not been shown.

The purpose of this study was to determine the feasibility and safety of creating precise histotripsy treatments within the superficial neck of a porcine thyroid model in

preparation for human clinical translation for the treatment of benign and possibly malignant thyroid tumors.

Materials and methods

Experimental design

The Institutional Animal Care and Use Committee (IACUC) approved all animal care and procedures for this study. Four healthy female pigs (approximately 55 kg, Arlington, WI) underwent histotripsy treatment in the superficial neck immediately followed by Magnetic Resonance Imaging (MRI). Animals were sacrificed immediately following imaging for necropsy and histopathology.

Animal model, handling and anesthesia

The intracervical pig thymus has been previously used as a model for the human thyroid in transoral thyroidectomy studies as well as for other neck surgeries [23,24]. The decision was made to use this model for the current study due to the location of the thymus overlying the diminutive porcine thyroid in the neck, as well as the similar depth, anatomic location, ultrasound appearance (Figure 1) and size compared to the human thyroid. The pig thyroid is too small (~5 ml) to be reproducibly targeted for histotripsy, and individual thyroid lobes are of insufficient size to contain a 1 cm histotripsy treatment [23].

Animals were sedated with an intramuscular injection of tiletamine and zolazepam (Telazol; Zoetis, Kalamazoo, MI), atropine (Phoenix Pharmaceutical, St. Joseph, MO), and xylazine (AnaSed, Shenandoah, IA). An intravenous catheter was placed in an auricular vein for administration of intravenous fluids and MRI contrast. Animals were positioned supine on a surgical table, intubated, and maintained under general anesthesia with inhaled isoflurane gas (1.5–2.5%, Halocarbon Laboratories, River Edge, NJ). Following completion of the MRI, animals were euthanized with an intravenous injection of phenobarbital sodium and phenytoin sodium (Beuthanasia-D; Schering-Plough, Kenilworth, NJ). A focused necropsy was then performed with removal of the anterior neck by a certified veterinary technician and radiologist.

Histotripsy

Histotripsy was performed using a research prototype system (HistoSonic, Inc., Ann Arbor, MI). The system consists of a 1 MHz therapeutic transducer (active aperture 4.6×7.1 cm, focal length 6.0 cm, and a working distance of 4.6 cm), a 3 degrees of freedom robotic delivery system and a co-axially aligned 4 MHz phased array diagnostic transducer for real-time continuous visualization, including targeting and monitoring the procedure. The therapy transducer was directed by a proprietary planning software package which can prescribe a treatment of virtually any size, shape, and volume [17,21,25].

Planning ultrasound was performed immediately prior to each treatment to identify an area within the thymus appropriate in size to fit the designated treatment and the overlying skin marked. In each animal a spherical $1.0 \times 1.0 \times 1.0$ cm (prescribed volume = 0.52 cm^3) and ovoid $1.0 \times 1.0 \times 2.0$ cm (prescribed volume = 1.046 cm^3) treatment was created in alternating lobes of the thymus. Treatment sizes were created to fit entirely within the thymus and be both spherical and ovoid to account for varying shapes of thyroid tumors. Once a region was chosen and localization of the planned treatment volume within the thymus confirmed with the coaxially-aligned diagnostic transducer, the acoustic power of the therapeutic transducer was increased incrementally, to an estimated in-situ peak negative pressure $>18 \text{ MPa}$, until a cavitation cloud was observed at the focal point in real-time by B-mode ultrasound. The treatment plan was defined, and the focal point moved through the planned treatment volume by the robot/software. Treatment progress was monitored by real-time B-mode ultrasound as a form of quality control, ensuring the cavitation cloud was observed within the planned treatment zone throughout the procedure. As there is real-time visualization of the treatment effect throughout the procedure, this was used to monitor for treatment throughout the planned volume and ensure targeting of sonications within the thyroid. Technical success was defined as the creation of a histotripsy treatment zone on post procedural MRI.

Magnetic resonance imaging

Multisequence, multiplanar MR imaging of the neck was performed with and without contrast immediately following completion of the procedure. MR images were obtained

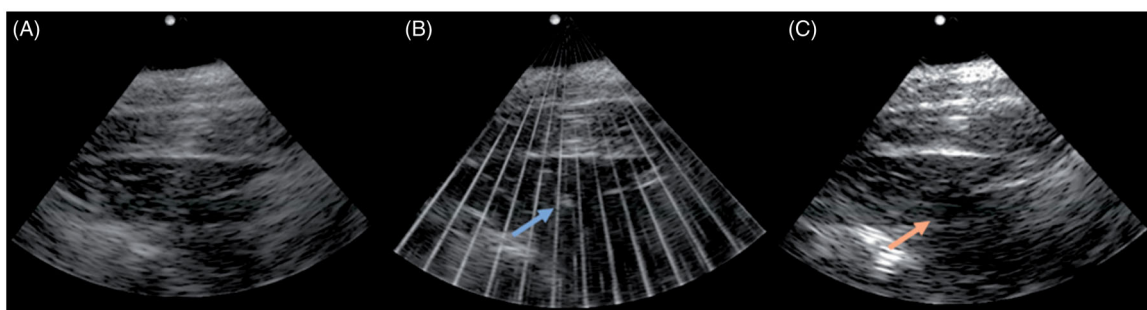


Figure 1. Axial US images pre (A), during (B), and post (C) histotripsy treatment of the targeted tissue in the anterior neck. The echogenic bubble cloud (blue arrow in B) is visible during histotripsy treatment for intraprocedural monitoring. Post procedure US image (C) demonstrates a hypoechoic treatment zone.

using a 3T MRI (Signa PET/MR, GE Healthcare, Waukesha, WI). Each animal received an intravenous injection of 0.25 ml/Kg gadobenate dimeglumine (MultiHance, Bracco Diagnostics, Wayne, NJ). MRI sequences included axial T2 fat-saturated fast spin echo (FSE), axial T2 short T1 inverse recovery (STIR), axial pre-contrast T1 fat-saturated FSE, axial post-contrast T1 fat-saturated, coronal post-contrast T1 IDEAL, axial and coronal post-contrast T1 LAVA-flex, axial diffusion weighted imaging (DWI), and axial apparent diffusion coefficient (ADC) with slice thickness ranging from 2.2 to 4.0 mm.

Imaging analysis

All MRI images were analyzed on a PACS workstation by three radiologists with 5–25 years of image interpretation experience. Images were evaluated for the treatment zone size, signal characteristics, presence of injury to the overlying skin and soft tissues, and abnormal imaging characteristics to adjacent organs, nerves and vessels to suggest injury. The T1 hypointense rim around each treatment was measured on axial and coronal post-contrast T1 LAVA-flex images (repetition time: 5.08 ms; echo time: 1.70 ms; flip angle: 15 degrees; matrix: 320 × 224; field of view: 380 mm; coil: body medium 5) with of 3.0 mm slice thickness. Measurements were made in the anteroposterior, transverse, and craniocaudal dimensions. Treatment zone volumes were calculated using a dedicated 3D reconstruction software package (Vitrea, Vital Images, Minnetonka, MN). The mean, (standard deviation), and 95% confidence intervals are reported for all measurements.

Histopathology

After the animals were euthanized, a focused necropsy was completed by a certified veterinary technician and radiologist. The entire anterior neck was removed, photographed, and fixed in 10% buffered formalin. The neck was sectioned along an axial plane similar to that of the MRI images for radiological-pathological correlation. The entirety of the histotripsy zone, the overlying skin and adjacent organs were sectioned and placed in cassettes. The tissues were then processed in a Sakura Tissue-Tek VIP (Sakura Finetek, Torrance, CA) and embedded with a Leica EG 1160 (Leica Biosystems, Richmond, IL). The sections were cut to 5 microns using a Leica RM2125RT (Leica Biosystems,

Richmond, IL) and stained with hematoxylin and eosin. The slides were interpreted by a pathologist with 7 years of clinical experience and 2 years of experience evaluating histotripsy specimens. Each zone was evaluated for percent cellular destruction as estimated by the pathologist and a measurement (cm) made at the transition between necrosis and normal tissue.

Results

Histotripsy successfully created treatment zones in 8/8 procedures for a technical success rate of 100%. The embedded diagnostic ultrasound system was able to visualize the echogenic bubble cloud throughout the entirety of the procedure in all cases (Figure 1). There were no procedural complications, skin injuries on physical examination or imaging, or evidence of physiologic distress on cardiopulmonary monitoring of the animals during or after treatment.

Treatment results

Each animal had a sphere (1.0 × 1.0 × 1.0 cm) and ovoid (1.0 × 1.0 × 2.0 cm) treatment zones successfully created in the superficial neck (Table 1). The mean depth of the treatment zone was 1.9 cm (range 1.3–2.2 cm), measured from the surface of the overlying skin to the superficial aspect of the treatment zone. Histotripsy treatment times were 8:22 for the sphere and 17:15 for the ovoid (see Table 1). By MRI, all treatment zones demonstrated measurements similar to the prescribed treatment. The mean actual sphere treatment diameter was 0.95 (0.10) cm in anteroposterior (AP; 95% CI 0.85–1.05 vs 1 cm), 0.95 (± 0.06) cm in transverse (TR; 95% CI 0.89–1.01 vs 1 cm), and 1.1 (± 0.00) cm in craniocaudal (CC; 95% CI 1.1 vs 1 cm) dimensions. The mean actual ovoid treatment diameters were 1.13 (± 0.13) cm in AP (95% CI 1–1.25 vs 1 cm), 1.23 (± 0.10) cm in TR (95% CI 1.13–1.32 vs 1 cm), and 2.0 (± 0.16) cm in CC (95% CI 1.84–2.16 vs 2 cm). The measured volumes of the histotripsy treatments closely matched the planned treatment volumes; actual volume 0.60 (± 0.11) cm³ vs 0.52 cm³ prescribed for the sphere, and actual volume 1.23 cm³ (± 0.40) vs 1.046 cm³ prescribed for the ovoid (Table 2). The prescribed volume of both the sphere and ovoid treatments were within the 95% confidence interval of the measured treatment zones (sphere: 95% CI 0.492–0.708 cm³ vs 0.52 cm³; ovoid 95% CI 0.838–1.62 cm³ vs 1.046 cm³). The actual treatment zone

Table 1. Description of histotripsy treatments.

Animal number	Prescribed treatment shape	Dimensions (AP × TR × CC cm)	Volume (cm ³)	Skin to superficial treatment distance (cm)	Percent cellular destruction (%)	Treatment time (min:sec)
1	Sphere	1.0 × 0.9 × 1.1	0.4	2	80–100	8:22
	Ovoid	1.1 × 1.1 × 1.8	0.8	2.1	80–90	17:15
2	Sphere	1.0 × 1.0 × 1.1	0.8	1.9	60–80	8:22
	Ovoid	1.1 × 1.3 × 2.2	1.8	2.2	50–60	17:15
3	Sphere	1.0 × 1.0 × 1.1	0.6	1.9	80–90	8:22
	Ovoid	1.3 × 1.3 × 2.0	1.1	2.1	50–90	17:15
4	Sphere	0.8 × 0.9 × 1.1	0.6	1.3	70–90	8:22
	Ovoid	1.0 × 1.2 × 2.0	1.2	1.9	50–95	17:15

AP: anteroposterior; TR: transverse; CC: craniocaudal.

Table 2. Actual treatment zone sizes vs prescribed ($n = 4$).

	Prescribed	Actual	Mean variation from prescribed value
Sphere			
Anteroposterior (cm)	1	0.95 ± 0.10	0.05
Transverse (cm)	1	0.95 ± 0.06	0.05
Craniocaudal (cm)	1	1.1 ± 0	0.1
Volume (cm ³)	0.52	0.6 ± 0.11	0.1
Ovoid			
Anteroposterior (cm)	1	1.13 ± 0.13	0.13
Transverse (cm)	1	1.23 ± 0.1	0.23
Craniocaudal (cm)	2	2.0 ± 0.16	0
Volume (cm ³)	1.046	1.23 ± 0.4	0.13

Data are measured in mean \pm standard deviation; n : number of measurements.

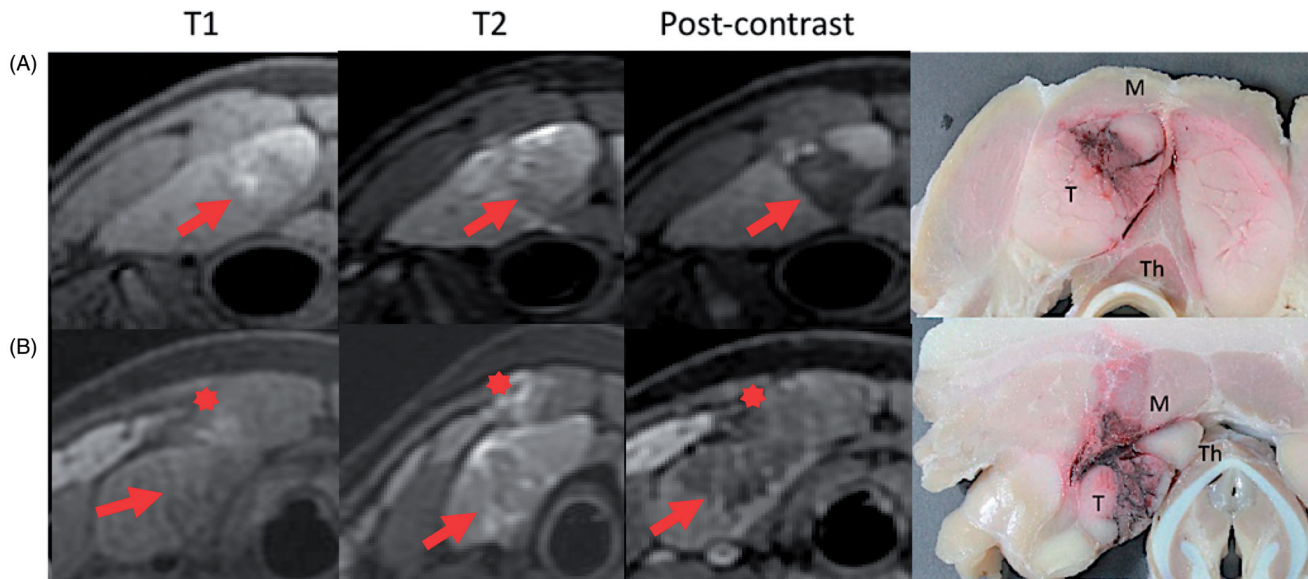


Figure 2. Post treatment MR (T1, T2 STIR, and T1 post-contrast) and gross pathology images from two experimental animals. Row A demonstrates observed histotripsy treatment changes including T2 hypointensity and non-enhancement of the treatment zone (arrow), with a rim of T2 hyperintensity around the treatment. Areas of intrinsic T1 intensity are likely due to blood products. Row B shows mild T2 intense edema (asterisk) and evidence of treatment effect in the overlying muscle (M). Gross images show treatment effects within the targeted thymus tissue (T). Note the diminutive thyroid gland (Th) deep to the thymus (T). Measurements were completed on MR images in anteroposterior, transverse, and craniocaudal dimensions.

volumes were 26% larger than the prescribed volume for the sphere and 22% larger for the ovoid.

Treatment characteristics on MRI

MRI images demonstrated well demarcated treatment zones, with thin transitions from treated to non-treated tissue (Figure 2). The treatment zones exhibited T2 hypointensity centrally, with areas of T2 hyperintensity around the treatment secondary to edema. T1 hyperintensity was present within the treatments, likely due to blood products from fractured red blood cells from histotripsy. Post-contrast images revealed a rim of T1 hypointensity outlining the treatments with non-enhancement within the treatment zone, suggestive of tissue necrosis. No diffusion restriction was seen in any of the treatment zones. All treatments demonstrated peripheral perfusional changes, including T1 arterial phase hypoenhancement. In two of eight treatments there was mild T2 hyperintensity in the musculature overlying the treatment zone, consistent with edema. This occurred in two separate animals, during the creation of one sphere and one ovoid treatment zone. The area of edema was located immediately superficial to the treatment zone. Both

of the areas of muscle edema demonstrated relatively normal enhancement on post-contrast images. No abnormal MR signal was identified within the overlying subcutaneous fat or skin, or within any organ adjacent to the treatments.

Histopathology

On histological review (Figure 3), a high degree of cellular destruction (mean 76% (± 12.5), range 50–100%) with a resultant acellular slurry was seen in the center of each treatment (Table 1). The zone of transition between areas of necrotic tissue and normal tissue outside the treatment zone was thin with a mean width of $0.33 (\pm 0.13)$ cm (range 0.2–0.5 cm). The transition zone demonstrated partial cellular destruction with hemorrhage and congestion within cells. Cellular swelling and interstitial edematous changes were identified in the muscle overlying treatment zones in 2/8 animals, correlating to those in which the T2 edema was noted on MRI (Figure 3). The muscle cell membranes remained intact with normal nuclei present. There was no evidence of treatment effect or change in any of the adjacent glandular tissue. Neurovascular bundles within the overlying muscle

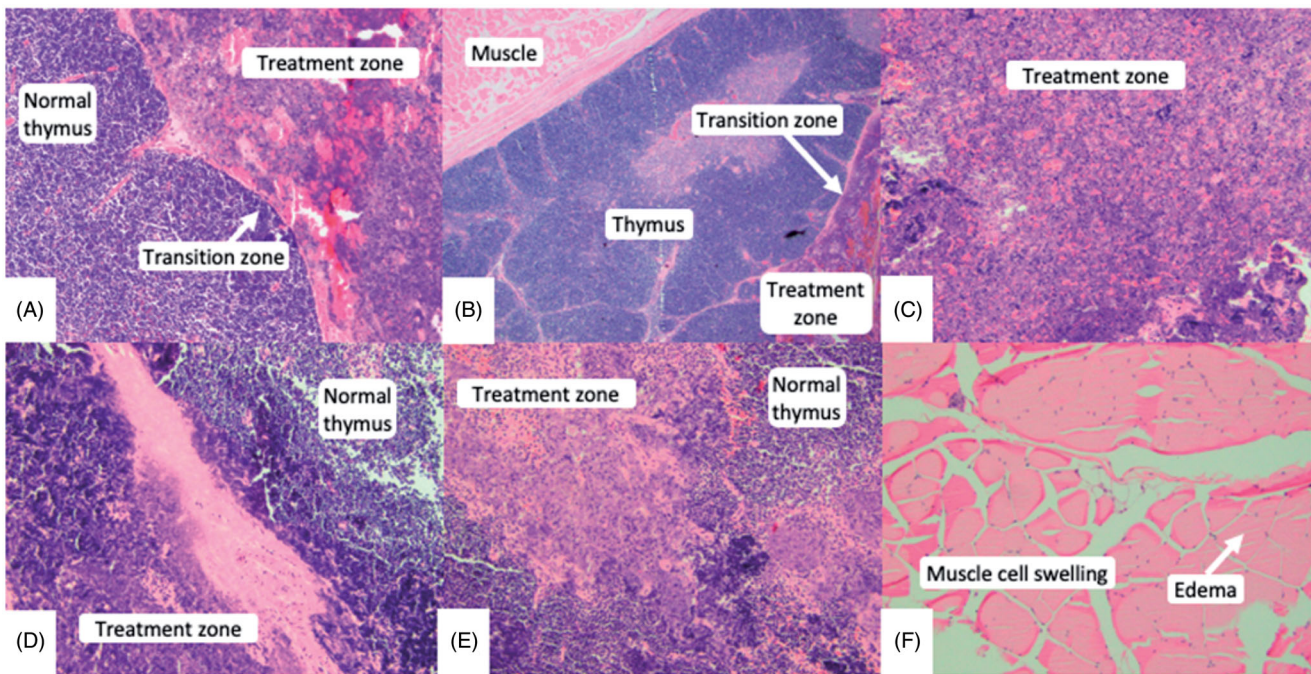


Figure 3. Microscopic images (hematoxylin and eosin) at 100 \times magnification. Thin transition zones (A & B) were seen between treated and normal tissue. Areas of complete and partial necrosis were seen within the treatment zone (C, D, E). Swollen muscle cells with interstitial edematous changes (E) were seen overlying two treatment zones, however their nuclei remained intact.

and tissues adjacent to the treatment zones were intact and demonstrated no treatment effect or change.

Discussion

The results of this *in vivo* proof of concept study demonstrate that it is possible to noninvasively and safely create histotripsy treatments in a human-scale live pig thyroid model. The treatment zones closely adhered to the prescribed size and shape, and had a high degree of targeted cellular destruction. Importantly, there was only minor edema seen within the overlying muscular tissue in two of eight cases. There was no evidence of injury to adjacent neurovascular bundles on MRI or pathology, no evidence of cardiopulmonary distress on physiologic monitoring, and no other complications during or immediately following treatment.

National guidelines suggest that minimally invasive techniques can be used to treat symptomatic benign nodules and for the treatment of thyroid cancer in some settings [5]. Minimally or noninvasive therapy options for treatment of benign and malignant thyroid nodules includes RFA, MWA, PEI, and thermal HIFU [11–13,26]. All currently available minimally-invasive therapies are associated with incomplete treatments and complications [11–13,26]. Specifically, RFA has shown therapeutic success ranges from 75% to 97% and a mean reduction of tumor volume of 8.4–50.9%, while PEI has shown therapeutic success ranges from 70.8% to 98% and a mean reduction of tumor volume of 37.5–96% [11]. Additionally, local cancer recurrence rates of 0–25% for RFA and 3.2–33% for PEI have been reported [11]. In this study there was incomplete treatment in the treatment zones with a variable amount of post-procedure viable tissue, ranging

from 50% to 100% in the treatment zone. In addition, the treatment volume exceeded that prescribed. These are likely a reflection of using a generic pulse path and treatment dose along with a transducer which was not of an optimal f number for treatment in the neck. In prior pig liver and kidney studies, there was complete necrosis of targeted tissue despite the increased depth and inferior ultrasound window [17,21,25]. It is expected that complete necrosis would be seen with either more pulses per treatment point (i.e., higher dose) or increased overlap between adjacent focal points, two parameters that are readily programmed into the treatment algorithm. For treatment of benign nodules, the destruction of every cell will be less important than for thyroid cancer, and so it is possible that two different strategies would ultimately be programmed into a clinical system. It's unlikely that the thymus model was an important reason for the residual viable cells seen in this study. Prior work has demonstrated that cellular tissue is vulnerable to treatment with histotripsy, and the degree of cellularity of the pig thymus and thyroid is similar [27]. Neither structure is composed of a high degree of fibrous tissue or a collagenous matrix, both of which are more resistant to damage from histotripsy compared to highly cellular organs or tumors [28,29].

Injury to the nerves within the anterior neck is a significant concern with currently available non/minimally invasive treatment options. Injury to the recurrent laryngeal nerve can cause voice changes and vocal cord paralysis, with voice complications seen in up to 6.2% of patients treated with RFA, 2.7% of patients treated with PEI, and 4% of patients treated with HIFU [9,11]. Importantly, no injury or treatment effect was seen within neurovascular bundles adjacent to treatment zones on MRI or pathology. RFA in particular has been shown to cause mild/moderate pain in the all patients,

as well as lower incidence of shoulder drop, hematomas, and skin burns due to the need for tissue puncture, lack of precision, and heating of vulnerable off-target tissues [12,26]. Histotripsy may have decreased complications in the adjacent nerves and glandular tissue due to the noninvasive and precise nature of the treatment. The rapid involution of treatment zones seen in prior studies may be an advantage in treatment of benign nodules for symptom relief or cosmesis [17,21]. No significant hemorrhage was identified on MRI or pathology post treatment. Bleeding has not been associated with histotripsy in multiple prior studies, even in anticoagulated animals, and it is expected that anticoagulation will not be a contraindication to histotripsy treatment in humans [17,21,25,30]. However, all of these potential advantages will ultimately need to be confirmed in a human clinical study.

Histotripsy is different than thermal HIFU in several important respects. HIFU directs high energy, high duty-cycle (ultrasound on-time/total treatment time >10%), ultrasound along a treatment path to create focal heating >60°C and tissue ablation at a small target [13]. While the highest temperatures are typically found at the focal point, tissue heating along the beam path is a substantial problem and can result in skin burns and collateral damage to vulnerable structures [31]. In contrast, histotripsy creates cavitation in the target tissue by directing high-amplitude, short ultrasound pulses to a focal point, while minimizing the heating using a low duty-cycle (<1%). Histotripsy is a binary threshold effect [27,32,33]. If the cavitation threshold of a particular tissue is not reached, there is no tissue damage, leading to highly precise treatments and minimal off-target damage [27,32,33]. Because of this, skin burns and collateral injuries are felt to be less likely with histotripsy than with HIFU [34]. In the current study, which employed a non-optimized therapy transducer and treatment protocol, there were no skin injuries, and only mild muscle edema immediately overlying the treatment in 2/8 cases. Previous histotripsy work within the liver (with a markedly inferior ultrasound window and deeper targets than the current study) demonstrated mild body wall edema which was eliminated with optimization of the treatment protocol for the liver [21,25]. Similar optimization of the treatment protocol, such as reduction of the time-average intensity of energy delivery, can be done and may eliminate any overlying edematous changes.

There are several limitations to the current proof of concept study. The thymus pig model used in this study was chosen due to its prior use in surgical studies as a thyroid surrogate, and a similar size, shape, cellularity and location compared to the human thyroid [23,24]. Prior *ex vivo* work on excised human tissue shows the potential for histotripsy to create effective thyroid treatment zones [27]. Importantly, there is the paucity of other human-scale readily translatable *in-vivo* animal thyroid models. Ideally, pig thyroid would have been used as a target, but it is too small to contain even a 1 cm treatment and is located deeper than in most humans—posterior to the upper border of the thymus and immediately superficial to the trachea (Figure 2). Human-scale thyroid nodule or cancer models are also not readily available. Other limitations include the relatively small

sample size and lack of longitudinal survival data to evaluate more than the most acute effects. Both of these choices were made as the study is intended as proof of concept with further work planned to increase cellular necrosis and decrease muscle injury prior to survival studies. Evaluating the evolution of the treatment zones, the transition zones, precision of treatment location, and edematous changes is needed, and will be a focus of future studies. Only two sizes and shapes of treatments were chosen, limited by the size of the pig thymus. On the technical side, a small aperture pediatric cardiac transducer was used for this study due to the ability to create a superficial treatment as well as to allow more optimal acoustic coupling and procedure workspace. The treatment protocol was also modified from prior work [17,21,25]. A multi-element purpose-built transducer with an iteratively designed treatment protocol could potentially improve the speed and efficacy of the treatment. However, despite the above limitations this study demonstrated the potential of histotripsy to create effective and highly precise treatments in a short period of time in a human-scale model.

In conclusion, histotripsy was able to create precise treatments in a human-scale porcine thyroid model without evidence of considerable collateral injuries in this proof of concept study. Additional research on histotripsy of the thyroid appears warranted to bring the technique closer to application in humans.

Acknowledgments

The authors appreciatively acknowledge the contributions of Jon Cannata Ph.D., Alex Duryea Ph.D., Ryan Miller Ph.D., for engineering and technical support, and Allison Rodgers, Jen Frank, Keri Graff for assistance in animal handling and cares.

Disclosure statement

JS, SM, EK, AZ, KL, XZ: No potential conflict of interest was reported by the author(s).

ZX: HistoSonics, Inc: founder, stockholder, paid consultant, research support.

PFL: HistoSonics, Inc: stockholder; Ethicon, Inc: paid consultant; Elucant Medical: paid consultant and stockholder; McGinley Orthopedic Innovations: stockholder; Siemens Medical: grant funding.

FTL: HistoSonics, Inc: Board of Directors, stockholder, research support; Medtronic Inc: patents, royalties; Ethicon, Inc: paid consultant.

TZ: HistoSonics, Inc: stockholder; Ethicon, Inc: paid consultant.

Study funded in part by:

HistoSonics, Inc., Ann Arbor, MI.

Funding

This work was supported by the HistoSonics, Inc.

ORCID

John F. Swietlik  <http://orcid.org/0000-0002-7180-794X>

Timothy J. Ziemlewicz  <http://orcid.org/0000-0002-7033-1062>

References

- [1] Ezzat S, Sarti DA, Cain DR, et al. Thyroid incidentalomas: prevalence by palpation and ultrasonography. *Arch Intern Med.* 1994; 154(16):1838–1840.
- [2] Guth S, Theune U, Aberle J, et al. Very high prevalence of thyroid nodules detected by high frequency (13 MHz) ultrasound examination. *Eur J Clin Invest.* 2009;39(8):699–706.
- [3] Reiners C, Wegscheider K, Schicha H, et al. Prevalence of thyroid disorders in the working population of Germany: ultrasonography screening in 96,278 unselected employees. *Thyroid.* 2004;14(11): 926–932.
- [4] American Cancer Society. Cancer facts & figures 2019. [Internet]. American Cancer Society; 2019 [cited 2020 Feb 1]. Available from: <https://www.cancer.org/content/dam/cancer-org/research/cancer-facts-and-statistics/annual-cancer-facts-and-figures/2019/cancer-facts-and-figures-2019.pdf>.
- [5] Haugen BR, Alexander EK, Bible KC, et al. 2015 American thyroid association management guidelines for adult patients with thyroid nodules and differentiated thyroid cancer: the american thyroid association guidelines task force on thyroid nodules and differentiated thyroid cancer. *Thyroid.* 2016;26(1):1–133.
- [6] Ho TWT, Shaheen AA, Dixon E, et al. Utilization of thyroidectomy for benign disease in the United States: a 15-year population-based study. *Am J Surg.* 2011;201(5):570–574.
- [7] Vassiliou I, Tympa A, Arkadopoulos N, et al. Total thyroidectomy as the single surgical option for benign and malignant thyroid disease: a surgical challenge. *Arch Med Sci.* 2013;9(1):74–78.
- [8] Erandes-Neto M, Tagliarini JV, López BE, et al. Factors influencing thyroidectomy complications. *Braz J Otorhinolaryngol.* 2012; 78(3):63–69.
- [9] Daher R, Lifante J-C, Voirin N, et al. Is it possible to limit the risks of thyroid surgery? *Ann Endocrinol (Paris).* 2015;76(1):1S16–1S26.
- [10] Promberger R, Ott J, Kober F, et al. Risk factors for postoperative bleeding after thyroid surgery. *Br J Surg.* 2012;99(3):373–379.
- [11] Jeong SY, Baek JH, Choi YJ, et al. Ethanol and thermal ablation for malignant thyroid tumours. *Int J Hyperthermia.* 2017;33(8): 938–945.
- [12] Korkusuz Y, Gröner D, Raczynski N, et al. Thermal ablation of thyroid nodules: are radiofrequency ablation, microwave ablation and high intensity focused ultrasound equally safe and effective methods? *Eur Radiol.* 2018;28(3):929–935.
- [13] Lang BH, Wu ALH. The efficacy and safety of high-intensity focused ultrasound ablation of benign thyroid nodules. *Ultrasonography.* 2018;37(2):89–97.
- [14] Parsons JE, Cain CA, Abrams GD, et al. Pulsed cavitation ultrasound therapy for controlled tissue homogenization. *Ultrasound Med Biol.* 2006;32(1):115–129.
- [15] Vlaisavljevich E, Kim Y, Allen S, et al. Image-guided non-invasive ultrasound liver ablation using histotripsy: feasibility study in an *in vivo* porcine model. *Ultrasound Med Biol.* 2013;39(8): 1398–1409.
- [16] Vlaisavljevich E, Maxwell A, Mancia L, et al. Visualizing the histotripsy process: bubble cloud-cancer cell interactions in a tissue-mimicking environment. *Ultrasound Med Biol.* 2016;42(10): 2466–2477.
- [17] Knott EA, Swietlik JF, Longo KC, et al. Robotically-assisted sonic therapy for renal ablation in a live porcine model: initial preclinical results. *J Vasc Interv Radiol.* 2019;30(8):1293–1302.
- [18] Maxwell AD, Owens G, Gurm HS, et al. Noninvasive treatment of deep venous thrombosis using pulsed ultrasound cavitation therapy (histotripsy) in a porcine model. *J Vasc Interv Radiol.* 2011; 22(3):369–377.
- [19] Schade GR, Keller J, Ives K, et al. Histotripsy focal ablation of implanted prostate tumor in an ACE-1 canine cancer model. *J Urol.* 2012;188(5):1957–1964.
- [20] Schuster TG, Wei JT, Hendlin K, et al. Histotripsy treatment of benign prostatic enlargement using the vortex R_x system: initial human safety and efficacy outcomes. *Urology.* 2018;114:184–187.
- [21] Smolock AR, Cristescu MM, Vlaisavljevich E, et al. Robotically assisted sonic therapy as a noninvasive nonthermal ablation modality: proof of concept in a porcine liver model. *Radiol Radiol Soc North Am.* 2018;287(2):485–493.
- [22] Sukovich JR, Cain CA, Pandey AS, et al. *In vivo* histotripsy brain treatment. *J Neurosurg.* 2018;1–8. DOI:10.3171/2018.4.JNS172652
- [23] Wilhelm T, Benhidjeb T. Transoral endoscopic neck surgery: feasibility and safety in a porcine model based on the example of thymectomy. *Surg Endosc.* 2011;25(6):1741–1746.
- [24] Wilhelm T, Klemm W, Leschber G, et al. Development of a new trans-oral endoscopic approach for mediastinal surgery based on ‘natural orifice surgery’: preclinical studies on surgical technique, feasibility, and safety. *Eur J Cardiothorac Surg.* 2011;39(6): 1001–1008.
- [25] Longo KC, Knott EA, Watson RF, et al. Robotically Assisted Sonic Therapy (RAST) for noninvasive hepatic ablation in a porcine model: mitigation of body wall damage with a modified pulse sequence. *Cardiovasc Intervent Radiol.* 2019;42(7):1016–1023.
- [26] Na DG, Lee JH, Jung SL, et al. Radiofrequency ablation of benign thyroid nodules and recurrent thyroid cancers: consensus statement and recommendations. *Korean J Radiol.* 2012;13(2):117–125.
- [27] Vlaisavljevich E, Kim Y, Owens G, et al. Effects of tissue mechanical properties on susceptibility to histotripsy-induced tissue damage. *Phys Med Biol.* 2014;59(2):253–270.
- [28] Macoskey JJ, Hall TL, Sukovich JR, et al. Soft-tissue aberration correction for histotripsy. *IEEE Trans Ultrason Ferroelectr Freq Control.* 2018;65(11):2073–2085.
- [29] Lake AM, Xu Z, Wilkinson JE, et al. Renal ablation by histotripsy—does it spare the collecting system? *J Urol.* 2008;179(3): 1150–1154.
- [30] Wheat JC, Hall TL, Hempel CR, et al. Prostate histotripsy in an anticoagulated model. *Urology.* 2010;75(1):207–211.
- [31] Lang BH-H, Wu ALH. High intensity focused ultrasound (HIFU) ablation of benign thyroid nodules – a systematic review. *J Ther Ultrasound.* 2017;5:11.
- [32] ter Haar G. Acoustic surgery. *Phys Today.* 2001;54(12):29–34.
- [33] Yu H, Burke CT. Comparison of percutaneous ablation technologies in the treatment of malignant liver tumors. *Semin Intervent Radiol.* 2014;31(2):129–137.
- [34] Kim Y, Vlaisavljevich E, Owens GE, et al. *In vivo* transcostal histotripsy therapy without aberration correction. *Phys Med Biol.* 2014; 59(11):2553–2568.